

# FINDING SINGULAR FEATURES

Christopher Genovese, Marco Perone-Pacifico,  
Isabella Verdinelli and Larry Wasserman  
Carnegie Mellon University and University of Rome

April 22 2016

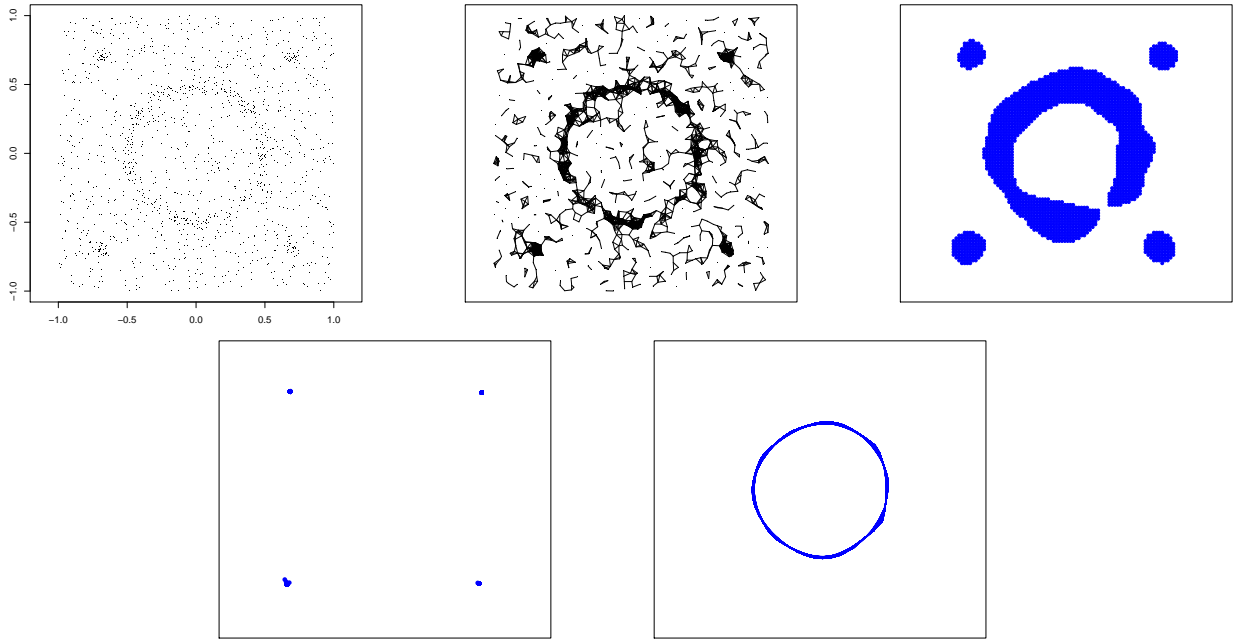
*We present a method for finding high density, low-dimensional structures in noisy point clouds. These structures are sets with zero Lebesgue measure with respect to the  $D$ -dimensional ambient space and belong to a  $d < D$  dimensional space. We call them “singular features.” Hunting for singular features corresponds to finding unexpected or unknown structures hidden in point clouds belonging to  $\mathbb{R}^D$ . Our method outputs well defined sets of dimensions  $d < D$ . Unlike spectral clustering, the method works well in the presence of noise. We show how to find singular features by first finding ridges in the estimated density, followed by a filtering step based on the eigenvalues of the Hessian of the density.*

**Keywords:** Clustering, Manifolds, Ridges, Density Estimation.

## 1 Introduction

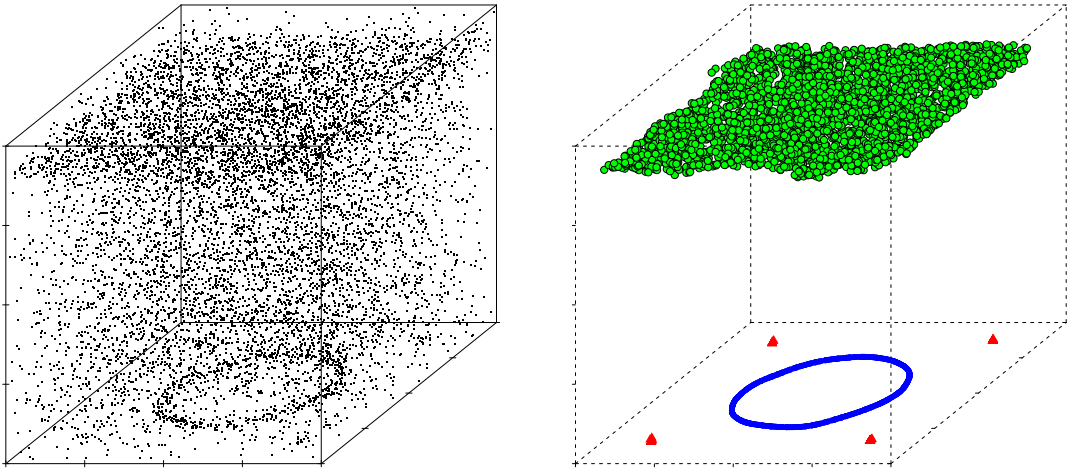
Let  $X_1, \dots, X_n \in \mathbb{R}^D$  be a sample from a distribution  $P$  with density  $p$ . We are interested in the question of finding salient features hidden in the  $\mathbb{R}^D$  space. We are looking for sets of arbitrary shape, with dimension  $d < D$ . The approach we take in this paper is based on an idea that we call *singular feature finding*. The idea is to find sets with high density but zero Lebesgue measure (with respect to  $\mathbb{R}^D$ ), that can be of dimension  $d \in \{0, 1, \dots, D - 1\}$ .

Figure 1 shows a simple two dimensional dataset. The top left plot shows the data. The top middle plot shows the result of standard single linkage clustering. Although this reveals some structure, the output is quite messy and hard to interpret. The top right plot shows an upper level set of the density estimate,  $\{\hat{p} > t\}$ . While this reveals the modes and ring, the output is two dimensional and the modes and ring are not well localized. The bottom row shows our singular feature finding method. The bottom left shows the singular features of dimension  $d = 0$ . The bottom right shows the singular feature of dimension  $d = 1$ .



**Figure 1.** Top left: raw data. Top middle: single linkage clustering. Top right: level set of density estimate Bottom: our method. Left: Dimension  $d = 0$  features. Right: Dimension  $d = 1$  feature.

The left plot in Figure 2 shows a three-dimensional dataset. The right plot shows high density structures hidden in the three dimensional point cloud. The structures are zero-dimensional (four modes marked as red triangles), one-dimensional (the blue ring at the



**Figure 2.** Left: raw data. Right: our algorithm extracts four 0-dimensional structures (modes), one 1-dimensional structure (a ring) and one 2-dimensional structure (plate) from the point cloud.

bottom) and two-dimensional (the wall at the top). These structures have high density but, as subsets of  $\mathbb{R}^3$ , they have zero Lebesgue measure.

In this paper we present a method for finding singular features. The method has the following steps:

1. Estimate the density.
2. Find the estimated *ridges*  $\widehat{R}_d$  of the density (or the log density) of dimension  $d = 0, 1, \dots, D - 1$ .
3. Filter out weak ridges: remove points from  $x \in \widehat{R}_d$  based on the eigenstructure of the Hessian of the density. The surviving points are denoted by  $\widehat{R}_d^\dagger$ .
4. Apply single linkage clustering to  $\widehat{R}_d^\dagger$  and, optionally, discard small connected components.

The four steps of our method are summarized in Figure 3. Note that even though  $\widehat{p}$  can be complex and unsmooth, the resulting singular feature is very smooth and simple.

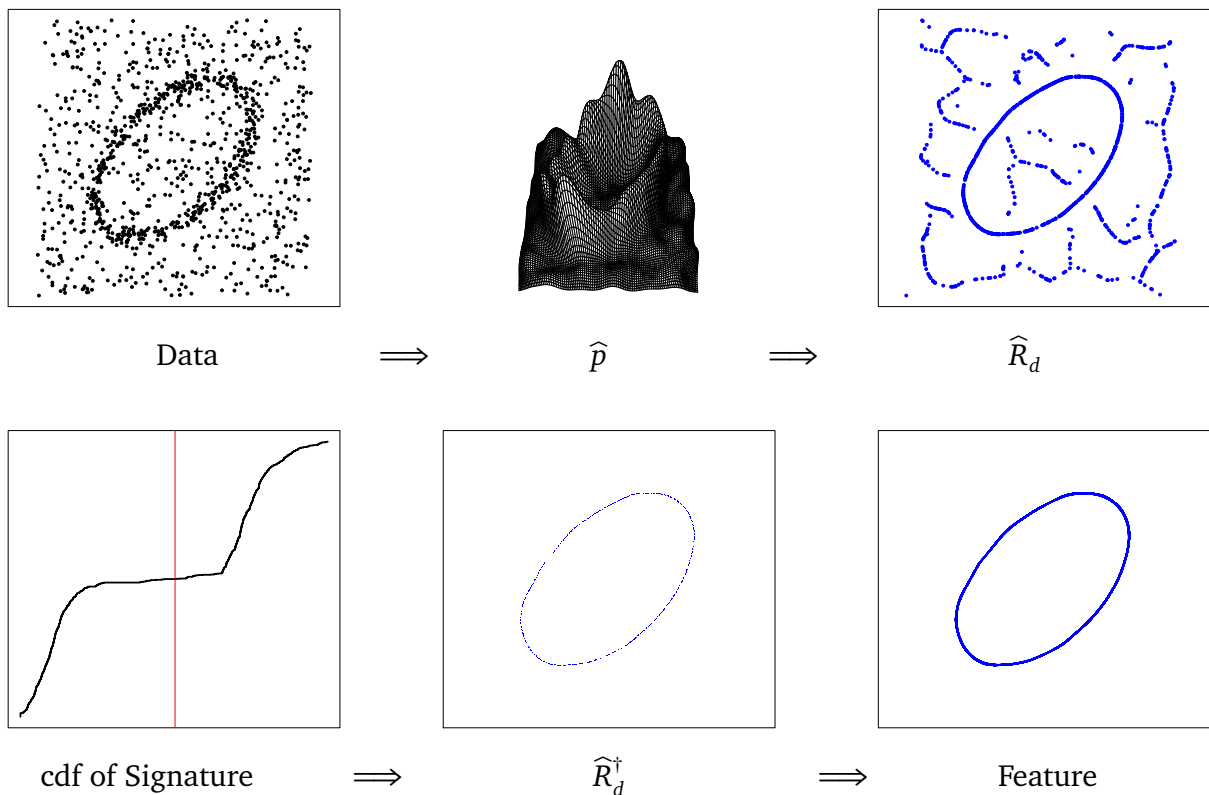


**Figure 3.** Steps of the algorithm. First we estimate the density then extract the ridge. Next we compute the signatures over the ridge. Based on the empirical cdf of the signatures (see section 4.5) we choose a threshold. Finally we apply single linkage clustering to the surviving points. Even though  $\widehat{p}$  can be complex and unsmooth, the resulting singular feature is very smooth and simple.

The first step uses kernel density estimation. The second step uses the subspace constrained mean shift (SCMS) algorithm due to Ozertem and Erdogmus (2011); see also Chen et al. (2015b) and Genovese et al. (2014). This algorithm finds density ridges  $\widehat{R}_d$  of dimension  $d$  for  $d = 0, 1, \dots, D - 1$ . The output of this step is a set (or collection of sets) of dimension  $d$ . In the third step, we use the eigenvalues of the estimated Hessian of the density to eliminate weak ridges. In the last step, we find the connected components using single linkage clustering and we eliminate the small components. What remains are large, high-density, lower dimensional structures.

*Related Work.* Mode finding is a special case of singular feature finding: modes of the density are zero dimensional singular features. There is a large literature on mode finding. It is impossible to list all the references here. Some useful recent references include (Klemela, 2009; Li et al., 2007; Dümbgen and Walther, 2008; Chacón, 2012; Genovese et al., 2015). Ridge theory has a long history in image processing; a standard reference is Eberly (1996). In the statistical context, ridges have been studied in Ozertem and Erdogmus (2011), Genovese et al. (2014), Chen et al. (2015b), Qiao and Polonik (2014). The idea of classifying structure based on the eigenvalues of the Hessian of the density has appeared in several places such as statistics, astronomy and image processing. A good astronomy reference is Cautun et al. (2013). Perhaps the work closest to ours in this regard is Godtlielsen et al. (2002). They estimate the density and then classify points into different types (valleys, ridges, etc) according to the eigenvalues of the Hessian. A critical difference with our approach is that our method separates structure by dimension.

A related idea is manifold learning. The literature on this topic is enormous. Some early key references are Tenenbaum et al. (2000); Roweis and Saul (2000). These methods are aimed at identifying structure when the data fall exactly on a sub-manifold which is quite different than the setting in this paper.

There is a large literature on spectral clustering which transforms the data using a kernel then performs some form of clustering. However, spectral methods do not work well in the presence of noise and they do not output structures of a given dimension  $d$ . We show an example in Section 5.

We would also like to mention some clustering methods aimed specifically at finding non-convex clusters. These include Amiri et al. (2015); Karypis et al. (1999); Zhong and Ghosh (2003). These methods find clusters in two stages, which allows them to find more general clusters than one can find with simpler methods such as  $k$ -means. For example, Zhong and Ghosh (2003) use  $k$ -means clustering (which tends to find spherical clusters) followed by post-processing that combines them into more general clusters. These methods appear to be effective at finding non-convex clusters. Their goal, however, is quite different than ours.

Another approach to finding structure is persistent homology; see Edelsbrunner et al. (2002); Edelsbrunner and Harer (2010); Frosini (1992); Turner et al. (2012); Bubenik and Kim (2007); Carlsson (2009); Carlsson and Zomorodian (2009); Chazal and Oudot (2008); Chazal et al. (2011); Cohen-Steiner et al. (2005); Edelsbrunner and Harer (2008); Ghrist (2008). Roughly

speaking, persistent homology looks for voids in the data. Singular feature finding, instead, seeks low dimensional, high density regions. In some cases, voids could be surrounded by high density ridges so it may be possible to connect ridge-based methods to persistent homology but we do not pursue that connection in this paper.

*Outline.* In Section 2 we give some mathematical background on modes and ridges. In Section 3 we formally define singular features. In Section 4 we show how to estimate the singular features. We consider some examples in Section 5. In Section 6 we study the asymptotic properties of the method. We conclude in Section 7 with some discussion.

## 2 Background: Modes and Ridges

We begin by reviewing mode finding (Klemela (2009); Li et al. (2007); Dümbgen and Walther (2008); Chacón (2012); Chen et al. (2014); Genovese et al. (2015)). Let  $p$  be a density on  $\mathbb{R}^D$  with gradient  $g$  and Hessian  $H$ . We assume that  $p$  is a Morse function meaning that the Hessian is non-degenerate at all critical points. Until Section 4, we assume that  $p$  is known.

A point  $m$  is a mode if  $\|g(x)\| = 0$  and the eigenvalues of  $H(x)$  are all negative. The *flow* starting at any point  $x$ , is a path  $\pi_x : \mathbb{R} \rightarrow \mathbb{R}^D$  such that  $\pi_x(0) = x$  and

$$\pi'_x(t) = \frac{d}{dt}\pi(t) = \nabla p(\pi_x(t)). \quad (1)$$

Then  $\pi_x$  is the steepest ascent curve starting at  $x$ . The destination of the path is defined by

$$\text{dest}(x) = \lim_{t \rightarrow \infty} \pi_x(t).$$

It can be shown that  $\text{dest}(x)$  is a mode, (except for  $x$  in a set of measure 0, whose paths lead to saddlepoints; Irwin (1980); Chacón (2012); Genovese et al. (2015)). Thus the modes can be thought of as the limits of gradient ascent paths. This observation leads to an algorithm for finding the modes of a kernel density estimator called the *mean shift algorithm* (Fukunaga and Hostetler (1975); Comaniciu and Meer (2002)). Mode finding is similar to level set estimation (Polonik (1995); Cadre (2006); Walther (1997)) but, in general, the two problems are not the same.

Now we turn to ridges. Let

$$\lambda_1(x) \geq \lambda_2(x) \geq \dots \geq \lambda_D(x) \quad (2)$$

denote the eigenvalues of  $H(x)$  and let  $\Lambda(x)$  be the diagonal matrix whose diagonal elements are the eigenvalues. Write the spectral decomposition of  $H(x)$  as  $H(x) = U(x)\Lambda(x)U(x)^T$ . Fix  $0 \leq d < D$  and let  $V(x)$  be the last  $D - d$  columns of  $U(x)$  (that is, the columns corresponding to the  $D - d$  smallest eigenvalues). If we write  $U(x) = [V_\circ(x) : V(x)]$  then we can write  $H(x) = [V_\circ(x) : V(x)]\Lambda(x)[V_\circ(x) : V(x)]^T$ . Let  $L(x) = V(x)V(x)^T$  be the projector on the linear space defined by the columns of  $V(x)$ . That is,  $V(x)V(x)^T$  projects onto the local normal space. Similarly,  $V_\circ(x)V_\circ(x)^T$  projects onto the local tangent space. Define the *projected gradient*

$$G(x) = L(x)g(x). \quad (3)$$

The ridge set  $R_d$  of dimension  $d$  is defined by

$$R_d = \left\{ x : \|G(x)\| = 0, \lambda_{D-d} < 0 \right\}. \quad (4)$$

The ridge set is geometrically like the ridge of a mountain: each point in  $R_d$  is a local maximum along a slice in the normal direction. Modes (0-dimension ridges) have  $D$  negative eigenvalues. One dimensional ridges are filaments and have  $D - 1$  negative eigenvalues. Two dimensional ridges are walls and have  $D - 2$  negative eigenvalues. And so on. By definition,

$$R_0 \subset R_1 \subset \dots \subset R_{D-1}. \quad (5)$$

Like modes, ridges are also the destinations of the paths but we replace the gradient field by the projected gradient vector field. Specifically, define  $\pi_x$  by  $\pi_x(0) = x$  and

$$\pi'_x(t) = G(\pi(t)). \quad (6)$$

The points in  $R_d$  are the destinations of these paths.

### 3 Singular Features

Ridge finding is a good start for finding structure. For example, it has been used successfully to map out the structure of matter in the Universe (Chen et al., 2015c). But ridges that are flat or small are not interesting. We want to find the portions of the  $d$ -dimensional ridges that are sharp and large. Also, as we explain later, ridges experience dimensional leakage: zero dimensional structure shows up in one dimension ridges and vice versa. In other words, ridge finding does not cleanly separate structure into objects of different dimensions. The next section shows how to find the sharp portion of the ridge.

#### 3.1 Sharpness

We quantify the sharpness of a ridge component by the eigenstructure of the Hessian  $H$ . The idea is to construct functions of the eigenvalues — called eigensignatures — that summarize the local shape of the density. In statistics, Godtliebsen et al. (2002), used the eigenstructure of  $H$  to classify points as belonging to different types of structure. Examples from the image processing literature include Descoteaux et al. (2004) and Frangi et al. (1998). In the astronomy literature, examples include the NEXUS signature due to Cautun et al. (2013) and the method in Snedden et al. (2014). Our use of the eigenstructure is somewhat different than these papers.

Let  $\lambda_1(x) \geq \dots \geq \lambda_D(x)$  be the eigenvalues of the Hessian  $H(x)$  of the  $\log p(x)$ . Let us also define  $\lambda_0(x) \equiv 0$ . The intuition of all eigensignature methods is based on the following

heuristic. In the *idealized case*, a  $d$ -dimensional structure would have the  $d$  smallest eigenvalues very negative and approximately equal. The remaining eigenvalues would be close to 0. For example, when  $D = 3$  we have the following idealized cases:

$$\begin{aligned} \text{mode } \lambda_3 \approx \lambda_2 \approx \lambda_1 < 0 \\ \text{filament } \lambda_3 \approx \lambda_2 < 0 \text{ and } \lambda_1 \approx 0 \\ \text{wall } \lambda_3 < 0 \text{ and } \lambda_2 \approx \lambda_1 \approx 0. \end{aligned}$$

Let us expand on this idealized case. Imagine a unimodal density with a spherical, sharply defined mode. In that case, the eigenvalues will all be negative and approximately equal, that is,  $\lambda_3 \approx \lambda_2 \approx \lambda_1 < 0$ . Now suppose that the mode is locally highly elliptical so that the density around the mode looks like a filament. In this case there will be two very negative eigenvalues but the largest eigenvalue will be close to 0. Thus,  $\lambda_3 \approx \lambda_2 < 0$  and  $\lambda_1 \approx 0$ . In the last case, suppose the density is very sharply concentrated around the mode in one dimension only and is otherwise very flat. Here, the density resembles a wall and we have  $\lambda_3 < 0$  and  $\lambda_2 \approx \lambda_1 \approx 0$ .

Now, we need to define functions of the eigenvalues that formalize these cases. We want a function  $S_0$  that is large when  $\lambda_3 \approx \lambda_2 \approx \lambda_1 < 0$ . Similarly, we want a function  $S_1$  that is large when  $\lambda_3 \approx \lambda_2 < 0$  and  $\lambda_1 \approx 0$ . And so on. To formalize this, we define the *eigensignatures*:

$$\begin{aligned} S_0 &= |\lambda_1| \frac{|\lambda_1|}{|\lambda_3|} I(\lambda_1 < 0) \\ S_1 &= |\lambda_2| \frac{|\lambda_2|}{|\lambda_3|} \left(1 - \frac{|\lambda_1 \wedge 0|}{|\lambda_3|}\right) I(\lambda_2 < 0) \\ S_2 &= |\lambda_3| \left(1 - \frac{|\lambda_1 \wedge 0|}{|\lambda_3|}\right) \left(1 - \frac{|\lambda_2 \wedge 0|}{|\lambda_3|}\right) I(\lambda_3 < 0) \\ &\vdots \end{aligned}$$

where  $I(\cdot)$  is the indicator function. More generally, for  $d = 0, \dots, D - 1$ :

$$S_j = I(\lambda_{j+1} < 0) |\lambda_{j+1}| \left(\frac{|\lambda_{j+1}|}{|\lambda_d|}\right) \prod_{i=0}^j \left(1 - \frac{|\lambda_i \wedge 0|}{|\lambda_d|}\right) \quad (7)$$

where we recall that  $\lambda_0 \equiv 0$ .

**Remark:** Note that, for simplicity, we have written  $S_j$  instead of  $S_j(x)$  and  $\lambda_j$  instead of  $\lambda_j(x)$ . We will often do this in what follows.

To get more intuition, consider the definition of  $S_0$ . Suppose that  $\lambda_3 \approx \lambda_2 \approx \lambda_1 < 0$ . Then the first term  $|\lambda_1|$  will be large and the second term  $|\lambda_1|/|\lambda_3|$  will be close to 1. Thus,  $S_0$  will be large. Now suppose  $\lambda_3 \approx \lambda_2 < 0$  and  $\lambda_1 \approx 0$ . In this case,  $|\lambda_1|/|\lambda_3|$  will be small, causing  $S_0$  to decrease. On the other hand, all the terms in  $S_1$  will be large. Hence, a filament-like structure will have  $S_0$  small and  $S_1$  large. Similar remarks apply to the higher order structures.

A large value of  $S_0$  thus suggests that  $x$  is a mode. A large value of  $S_1$  suggests that  $x$  is a one-dimensional ridge point and so on. In particular, given a threshold  $T_d$ , we call

$$R_d^\dagger = \{x \in R_d : S_d(x) > T_d\}$$

the sharp portion of the ridge. In Section 4.5 we explain how to choose the threshold  $T_d$ .

To explore the eigensignature further, Figure 4 shows some stylized cases.

	$\lambda_3$	$\lambda_2$	$\lambda_1$	$S_0$	$S_1$	$S_2$
mode:	$-C$	$-C$	$-C$	$C$	$0$	$0$
filament:	$-C$	$-C$	$0$	$0$	$C$	$0$
wall:	$-C$	$0$	$0$	$0$	$0$	$C$

**Figure 4.** Examples of signatures. The first three entries of each row show a configuration of the eigenvalues of the Hessian.  $C > 0$  is any positive constant. The last three entries show the corresponding values of the signature  $S = (S_0, S_1, S_2)$ .

Some more varied cases are shown Figure 5. The left plot of Figure 5 shows that when there

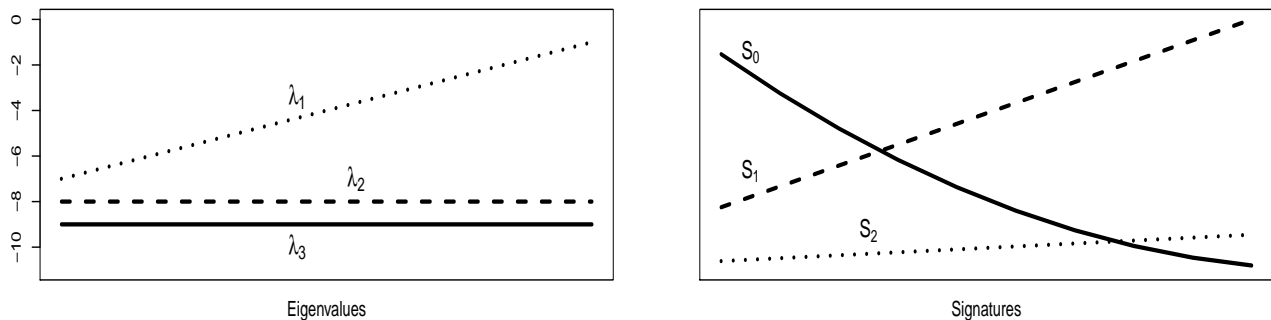


**Figure 5.** Left: The evolution from mode to filament. Left: eigenvalues. Solid line:  $\lambda_1$ , broken line:  $\lambda_2$ , dotted line:  $\lambda_3$ . Right: signatures. Solid line:  $S_0$ , broken line:  $S_1$ , dotted line:  $S_2$ .

are three, negative, tightly clustered eigenvalues,  $S_0$  is large. As we increase the largest eigenvalue (which corresponds to moving up higher in the left plot) we see that  $S_0$  decreases and  $S_1$  increases. Thus, two negative, clustered eigenvalues and one larger eigenvalue is declared to be more filament-like.

## 4 Estimating Singular Features

So far, our discussion has referred to the true density  $p$ . To find singular features in point clouds, we need to estimate all the relevant quantities.



## 4.1 Estimating The Density

To estimate the density  $p$ , we use the standard kernel density estimator

$$\hat{p}_h(x) = \frac{1}{n} \sum_{i=1}^n \frac{1}{h^D} K\left(\frac{\|y - X_i\|}{h}\right) \quad (8)$$

where  $K$  is a smooth, symmetric kernel and  $h > 0$  is the bandwidth.

We use the multivariate form of Silverman's Normal reference rule to choose the bandwidth  $h$ . For a matrix-valued bandwidth, Chacón et al. (2011) show that this is

$$H = \left(\frac{4}{n(d+2)}\right)^{\frac{2}{4+d}} S$$

where  $S$  is an estimate of the covariance matrix. For simplicity we use a scalar bandwidth

$$h = \left(\frac{4}{n(d+2)}\right)^{\frac{1}{4+d}} s \quad (9)$$

where  $s^2 = D^{-1} \sum_{j=1}^D s_j^2$ , and  $s_j$  is the standard deviation of the  $j^{\text{th}}$  coordinate.

**Remark:** This choice of bandwidth has the optimal rate for estimating  $p$  under standard smoothness assumptions. However, estimating the ridges involves estimating the gradient and Hessian as well as the density. In principle, we could use separate bandwidths for estimating the gradient and the Hessian. However, to keep the method simple, we suggest using a single bandwidth even if it is not optimal.

## 4.2 Estimating the Ridge

Let  $\hat{H}(x)$  be the Hessian of  $\hat{p}(x)$  and let

$$\hat{\lambda}_1(x) \geq \hat{\lambda}_2(x) \geq \dots \geq \hat{\lambda}_D(x) \quad (10)$$

denote the eigenvalues of  $\hat{H}(x)$ . Write the spectral decomposition of  $\hat{H}(x)$  as

$$\hat{H}(x) = \hat{U}(x) \hat{\Lambda}(x) \hat{U}(x)^T$$

and let  $\hat{V}(x)$  be the last  $D - d$  columns of  $\hat{U}(x)$  (that is, the columns corresponding to the  $D - d$  smallest eigenvalues). Write  $\hat{U}(x) = [\hat{V}_s(x) : \hat{V}(x)]$  and let  $\hat{L}(x) = \hat{V}(x) \hat{V}(x)^T$  be the projector on the linear space defined by the columns of  $\hat{V}(x)$ . The plugin estimate of the projected gradient is  $\hat{G}(x) = \hat{L}(x) \hat{g}(x)$  where  $\hat{g}$  is the gradient of  $\hat{p}$ . The estimated ridge set  $\hat{R}_d$  is

$$\hat{R}_d = \left\{ x : \|\hat{G}(x)\| = 0, \hat{\lambda}_{D-d} < 0 \right\}. \quad (11)$$

The properties of  $\widehat{R}_d$  are studied in Chen et al. (2015a), Chen et al. (2015b) and Genovese et al. (2014). In particular, Genovese et al. (2014) showed that the estimated ridges consistently estimate the true ridges. Chen et al. (2015b) established the limiting distribution of the estimated ridge which leads to a method for constructing confidence sets.

In practice, we replace  $\widehat{R}_d$  with a numerical approximation based on the subspace constrained mean shift (SCMS) algorithm due to Ozertem and Erdogmus (2011). Before explaining the SCMS algorithm, it is helpful to first review the basic mean shift algorithm (Fukunaga and Hostetler (1975); Comaniciu and Meer (2002)). This is a method for finding the modes of a density by approximating the steepest ascent paths. The algorithm starts with a mesh of points and then moves the points along gradient ascent trajectories towards local maxima.

Recall that  $\widehat{p}_h(x)$  denotes the kernel density estimator. Let  $\mathcal{M} = \{m_1, \dots, m_N\}$  be a collection of mesh points. These are often taken to be the same as the data but in general they need not be.

Let  $m_j(1) = m_j$  and for  $t = 1, 2, 3, \dots$  we define the trajectory  $m_j(1), m_j(2), \dots$ , by

$$m_j(t+1) = \frac{\sum_{i=1}^n X_i K\left(\frac{\|m_j(t) - X_i\|}{h}\right)}{\sum_{i=1}^n K\left(\frac{\|m_j(t) - X_i\|}{h}\right)}. \quad (12)$$

It can be shown that each trajectory  $\{m_j(t) : t = 1, 2, 3, \dots\}$  approximates the gradient ascent path and converges to a mode of  $\widehat{p}_h$ . Conversely, if the mesh  $\mathcal{M}$  is rich enough, then for each mode of  $\widehat{p}_h$ , some trajectory will converge to that mode. The mean shift algorithm is simply a numerical approximation to the flow defined by (1). This was recently made rigorous in Arias-Castro et al. (2013). The mean shift algorithm is simply a mode-finding algorithm. In fact, it can be shown that the mean shift algorithm is just a type of gradient ascent. Given any starting value  $x$ , the algorithm keeps moving the point in the direction of the gradient towards a local maximum.

The SCMS algorithm mimics the mean shift algorithm but it replaces the gradient with the projected gradient at each step. The algorithm can be applied to  $\widehat{p}$  or any monotone function of  $\widehat{p}$ , such as  $\log \widehat{p}$ , in Figure 6. The SCMS algorithm can also be regarded as a gradient ascent algorithm. Starting from a point  $x$ , the algorithm moves the point in the direction of the gradient. However, we want the point to move towards a ridge rather than a mode. To accomplish this, SCMS takes the point and then projects into the space, perpendicular to the ridge. This forces the point to move towards the ridge and stop, rather than moving up the ridge towards a mode. The details are formalized in Ozertem and Erdogmus (2011).

### SCMS Algorithm

1. Input:  $q(x) = \log \hat{p}(x)$  and a mesh of points  $M = \{m_1, \dots, m_N\}$ .
2. Let  $g(x)$  and  $H(x)$  be the gradient and Hessian of  $q$ .
3. Let  $V = [v_1 \cdots v_{D-d}]$  be the  $D \times (D-d)$  matrix whose columns are the eigenvectors of  $H(x)$  corresponding to the smallest  $D-d$  eigenvalues.
4. For each mesh point  $m$  repeat:

$$m \leftarrow m + VV^T \left( \frac{\sum_i c_i X_i}{\sum_i c_i} - m \right)$$

where  $c_i = h^{-D}K(\|m - X_i\|/h)$ .

5. Stop when convergence is obtained.

**Figure 6.** The SCMS algorithm of Ozertem and Erdogmus (2011).

Figure 7 shows a simple dataset with the outputs  $S_0$  and  $S_1$  of SCMS for  $d = 0$  and 1. The left plot shows the data, the middle plot shows  $\hat{R}_0$  and the right plot shows  $\hat{R}_1$ . Here we see an effect that we call *dimensional leakage*. The set  $\hat{R}_0$  contains some ridge points (since ridge points can also be local modes). Similarly,  $\hat{R}_1$  contains the modes; this must happen since, by definition,  $R_0 \subset R_1 \subset R_2 \cdots$ . This is why filtering with the eigensignature is helpful.

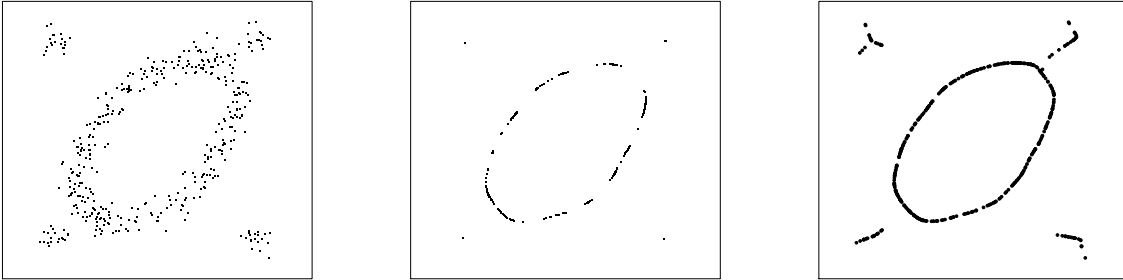


**Figure 7.** Dimensional leakage. Left: Data. Center:  $SCMS_0$  contains the true modes but also false modes from the oval. Right:  $SCMS_1$  contains the true oval but also false ridges from the modes.

In principle, we could use a very fine grid of starting values and trace out  $\hat{R}_d$  very accurately. But this is time consuming and in practice we have found that using the data points as starting values leads to an accurate approximation of the ridge. Thus, let  $Y_i$  be the destination of SCMS after running the algorithm with the data point  $X_i$  as a starting point. We use  $\hat{R}_d = \{Y_i : i = 1, \dots, n\}$  as our estimate of the ridge.

### 4.3 Estimating the Signature

We use the plug-in estimator for the signatures. Thus, we take  $\widehat{H}(x)$  to be the Hessian of  $\log \widehat{p}(x)$  and we let  $\widehat{\lambda}_j(x)$  be the eigenvalues of  $\widehat{H}(x)$ . Then we estimate the signature by

$$\widehat{S}_j = I(\widehat{\lambda}_{j+1} < 0) |\widehat{\lambda}_{j+1}| \left( \frac{|\widehat{\lambda}_{j+1}|}{|\widehat{\lambda}_d|} \right) \prod_{i=1}^j \left( 1 - \frac{|\widehat{\lambda}_i \wedge 0|}{|\widehat{\lambda}_d|} \right) \quad (13)$$

Having estimated the signature, we estimate the sharp ridge by

$$\widehat{R}_d^\dagger = \left\{ Y_i \in \widehat{R}_d : \widehat{S}_d(Y_i) > T_d \right\}. \quad (14)$$

### 4.4 Connected Components: Single Linkage Clustering (The Rips Graph)

The sets  $\widehat{R}_d^\dagger$  can be used as the final output of the procedure. However, in some cases, the user may want to summarize  $\widehat{R}_d^\dagger$  as a collection of connected components.

Let us write  $\widehat{R}_d^\dagger = \{Y_1, \dots, Y_m\}$  say. The Rips graph is defined as follows. Each node in the graph corresponds to a point  $Y_i \in \widehat{R}_d^\dagger$ . We put an edge between two nodes  $Y_i$  and  $Y_j$  if and only if  $\|Y_i - Y_j\| \leq \epsilon$ . The connected components of the Rips graph are precisely the clusters obtained

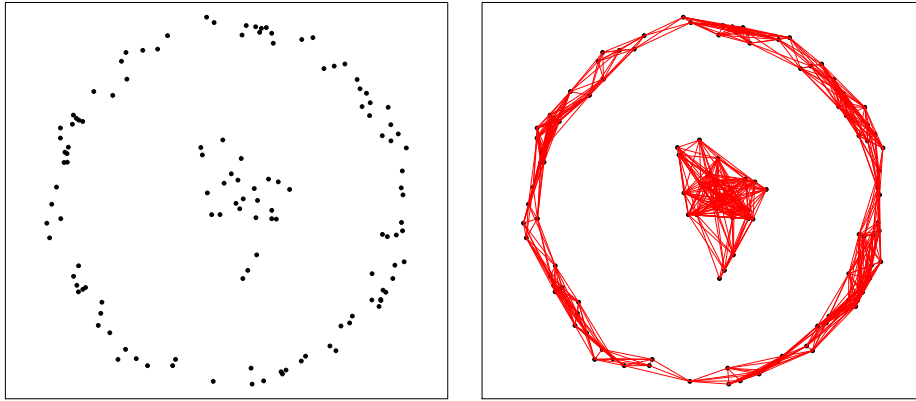


**Figure 8.** Left: A two-dimensional data set. Right: the Rips graph. Every pair of points  $X_i$  and  $X_j$  such that  $\|X_i - X_j\| \leq \epsilon$  is connected.

by performing single linkage clustering and then cutting the dendrogram at height  $\epsilon$ . Let  $\widehat{R}_{d1}^\dagger, \dots, \widehat{R}_{d\ell}^\dagger$  denote the connected components of the graph (i.e. the single linkage clusters). Figure 8 shows a Rips graph.

Optionally, we may also want to discard small components. Thus we can discard a connected component if  $n_j \geq N_d$  where  $n_j$  is the number of data points that ended up in component  $\widehat{R}_{dj}^\dagger$  and  $N_d$  is a user-chosen constant. The tuning parameter  $\epsilon$  is discussed in Section 4.5.

## 4.5 Choosing the Tuning Parameters

Here we provide suggestions for choosing all the tuning parameters. Our suggestions are meant to be simple and transparent. We make no claim that they are optimal. Singular feature finding is an exploratory method and the user is encouraged to try different tuning parameters. Our suggestions can be used as starting points.

1. *The Bandwidth  $h$ .* Our default is given in equation (9). (In some cases, we have found that using  $h/2$  can improve the performance.)
2. *The Signature Threshold  $T_d$ .* A simple method that we have found very effective is to plot a histogram of the signature values and choose  $T_d$  to be at a minimum. Alternatively, we plot the empirical cdf of the signature values and choose  $T_d$  to be in a flat spot of the cdf. Specifically, we compute the signature at each data point and we find the empirical cdf of these numbers (as in Figure 3). We illustrate this method in Section 5. It would not be difficult to automate this method. For example, fit a one dimensional kernel estimator to the signatures and choose the rightmost local minimum. In practice, choosing it by visually inspecting the cdf works very well.

An alternative, and more formal approach, is to use a null distribution. We assume that the data are a sample of size  $n$  from a distribution on a known, compact set  $\mathcal{X}$ . (Otherwise, the data can be truncated to some compact set.) Draw  $U_1, \dots, U_n$  from a uniform distribution  $\mathbb{U}$  on  $\mathcal{X}$ . We regard  $\mathbb{U}$  as a null distribution. We run the SCMS algorithm on these points (using the same bandwidth  $h$  that is used on the real data) and we compute the estimated signatures. Let  $\tau_d$  be the maximum value of the signatures. This process is repeated many times to get an estimate of the cdf

$$F_d(t) = \mathbb{U}(\tau_d \leq t)$$

where  $\mathbb{U}$  indicates that we are using the uniform distribution. This defines, in a sense, a null distribution for the maximum signature. One can use an upper quantile of  $F_d$  as the threshold  $T_d$ . This Monte-Carlo approach is simple but time consuming.

3. *The Rips Parameter  $\epsilon$ .* In Section 4.4 we used a parameter  $\epsilon$  for the Rips graph. As above, let  $U_1, \dots, U_n$  be  $n$  draws from a uniform distribution on  $\mathcal{X}$ . Let  $U'_i$  be the nearest neighbor to  $U_i$ . We suggest setting

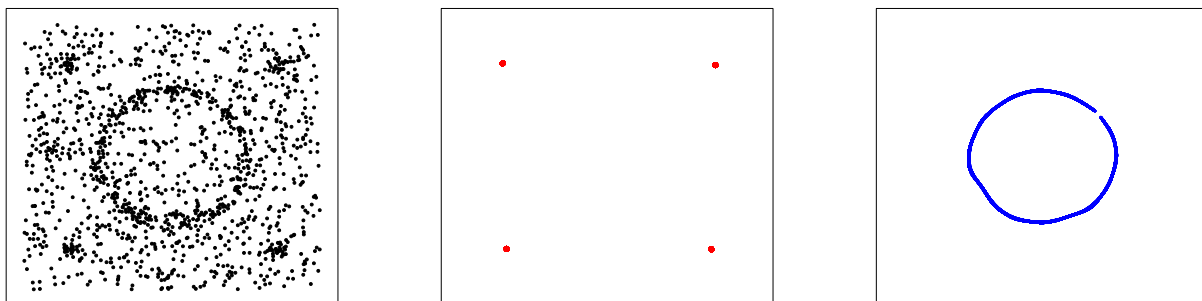
$$\epsilon = \mathbb{E}\|U_i - U'_i\|.$$

The parameter  $N_d$  can be chosen subjectively or omitted entirely. Alternatively, let  $N$  be the size of the largest connected component of the Rips graph on the uniform data using threshold  $\epsilon$ . The null simulation gives the distribution  $G(t) = \mathbb{U}(N \leq t)$ . We can then choose an upper quantile of  $G$ . An alternative is to start with a small  $\epsilon$  and then increase  $\epsilon$  until the number of connected components stabilizes.

## 5 Examples

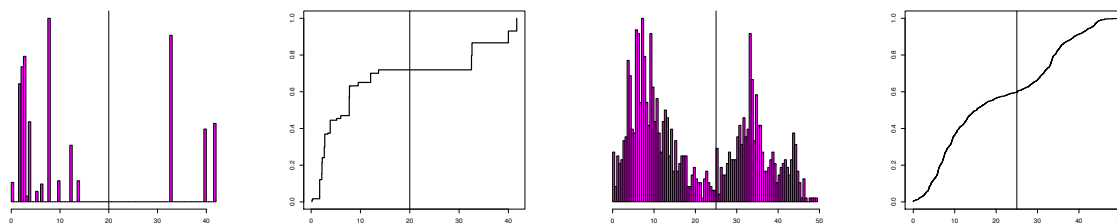
### 5.1 Two-dimensional Example.

Fig 9 shows an example of a two dimensional dataset hiding five singular features. Our method finds four 0-dimensional features (modes) and one 1-dimensional feature (filament).



**Figure 9.** *Two Dimensional example. This plot shows a two-dimensional dataset and the 0- and 1-dimensional singular features found with our method.*

In Figure 10 we plot histograms and empirical cdf's of 0- and 1-dimensional signatures, together with their thresholds  $T_d$  ( $d = 1, 2$ ) determined by the null distribution approach.



**Figure 10.** *Two Dimensional example. The four plots are the signatures' histogram and cdf for 0-dimensional (two left plots) and 1-dimensional (two right plots) singular features. The vertical lines in the four plots are the signature thresholds  $T_d$  for  $d = 0$  and  $d = 1$*

### 5.2 Three-Dimensional Example.

This example is similar to the plots shown in Figure 2, but finding the hidden one-dimensional structure is more challenging. The five singular features hidden in the dataset were found using the threshold with the null distribution approach.

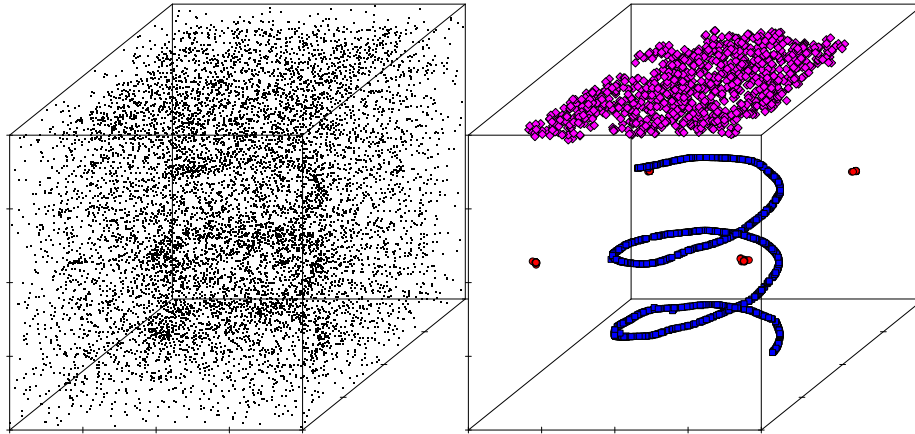


**Figure 11.** *Left: Dataset Right: our algorithm extracts four 0-dimensional structures (modes), one 1-dimensional structure (a corkscrew) and one 2-dimensional structure (plate) from the point cloud.*

### 5.3 Spectral Clustering Example

In Figure 12 we analyze the data from the example in 5.1 using spectral clustering. There are many different versions of spectral clustering. We use the default method in the R package kernlab. The left plot shows a dataset with no noise. The colors correspond to the clusters. In this case, the clustering is perfect.

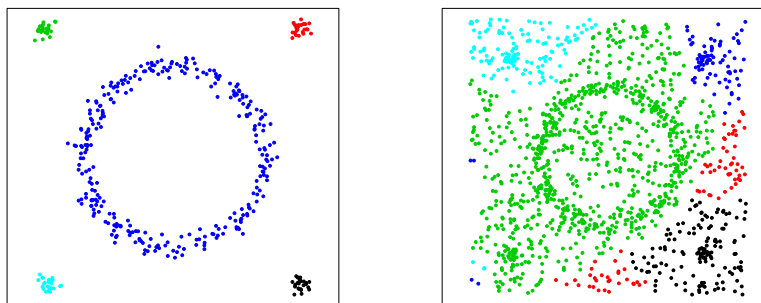


**Figure 12.** *Spectral clustering applied to the data from Example 1. The left plot shows a dataset with no noise. The colors correspond to the clusters. In this case, the clustering is perfect. The right plot shows what happens when we add noise. In this case spectral clustering fails.*

The right plot shows what happens when we add noise. In this case, spectral clustering fails. In both cases, the output is two dimensional; spectral clustering does not output zero or one dimensional features. Also, we had to specify the correct number of clusters by hand. Thus we see several advantages of singular feature finding; it handles noise, it separates clusters by dimension, and it does not require that we specify the number of clusters.

## 5.4 Intersecting Curves

Figure 13 shows an interesting example from Arias-Castro, Lerman and Zhang (2103). The data, shown in the top left plot, fall on two intersecting curves. The distribution is in fact singular.

Arias-Castro, Lerman and Zhang (2103) develop a method based on local PCA for analyzing such data. Here we are interested in what happens if we apply singular feature finding. We focus on  $d = 1$  as this is obviously the case of interest here. The top middle plot shows that the method

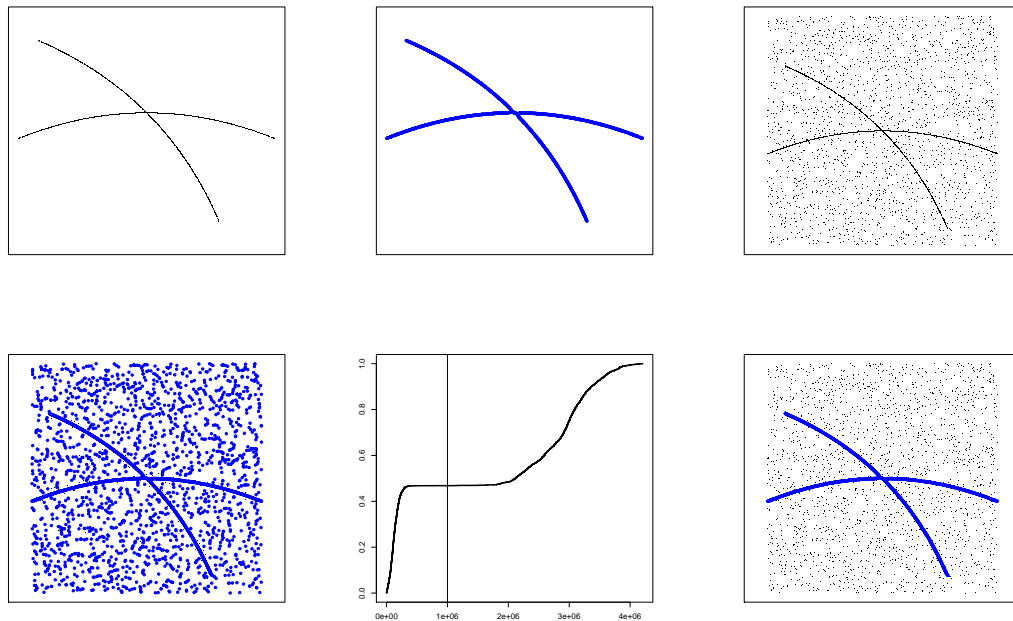


**Figure 13.** *The Intersecting Curves Examples. TOP Left: noiseless data. Middle: the resulting singular feature. Right: noisy data. BOTTOM. Left: singular feature without signature thresholding. Note the many spurious points (dark dots), identified as dimension zero features. Middle: cdf of the signatures. Right: singular feature after thresholding. Here the noise points (light dots) are included in the plot but they are not part of  $\widehat{R}_1^+$ .*

returns a single feature which follows the data quite closely. It is not obvious from the plot but there is a small bias at the intersection. Choosing the bandwidth slightly smaller than the Silverman rule reduces this bias. In fact, the local PCA method of the aforementioned authors avoids this bias as it was designed for datasets of this form. Nevertheless, singular feature finding works quite well. Next we add noise as shown in the top right plot. If we blindly apply singular feature finding we get the main cluster plus many modes as shown in the bottom left plot. The bottom middle plot shows the cdf of the signatures. There is a clear flat spot in the cdf and if we threshold at some value in this zone we get the feature shown in the bottom



right plot. Thus, singular feature finding with signature thresholding work very well. Note that the noise points (light dots) are included in the last plot but they are not part of  $\widehat{R}_1^\dagger$ .

## 5.5 Mt. St. Helens Earthquake Dataset

Figure 14 shows the Mt. St. Helens earthquake data, taken from Scott (1992), Scott (2015), and Duong et al. (2008). The data are available at <http://www.stat.rice.edu/~scottdw/ALL.DATASETS/earthquake>.

The data consist of measurements of the epicentres of 510 earthquakes which took place beneath the Mt. St. Helens volcano before its 1982 eruption. As in Duong et al., we take the first three variables longitude (degrees), latitude (degrees) and depth (km), from the full set of 5 variables. Following Scott, the depth variable  $z$  is transformed to  $-\log(-z)$ , where negative depths indicate distances beneath the Earth's surface.

Figure 14 shows the 3-dimensional data set together with the detected singular features. We found three singular features of dimension 0 (maxima) and two singular features of dimension 1 (filaments). The filaments shown in the right plot suggest the existence of a depth fault-line in the data. We did not find any singular feature of dimension 2.

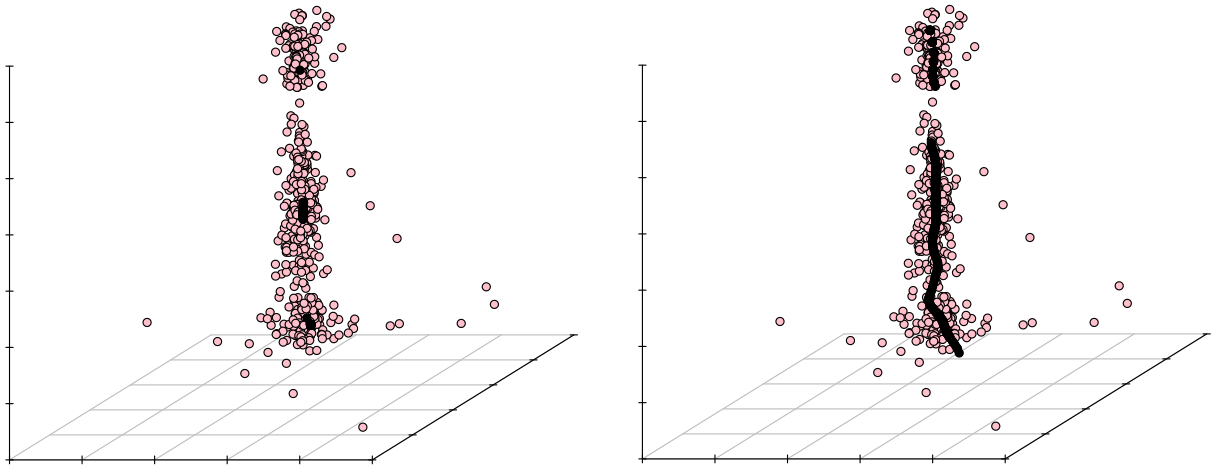


**Figure 14.** Mt. St. Helen hearthquakes. Longitude is shown on the x-axis, latitude on the y-axis, and depth on the z-axis. Left: black dots show singular features of dimension  $d = 0$ . Right: black dots show singular features of dimension  $d = 1$ . Singular features of dimension  $d = 2$  were not found.

## 5.6 Voronoi Foam

Voronoi foam models are simulations models invented in Icke and van de Weygaert (1991); van de Weygaert (1994); van de Weygaert and Schaap (2009). These models are meant to mimic astronomical galaxy surveys by having a mixture of modes, filaments, walls and noise.

The data are created as follows. We select  $N$  random points in the cube  $[-1, 1]^3$ . We then form the Voronoi partition defined by these points. The partition is a set of polygons which intersect at points, lines and walls. Random points are added at these points, lines and walls.

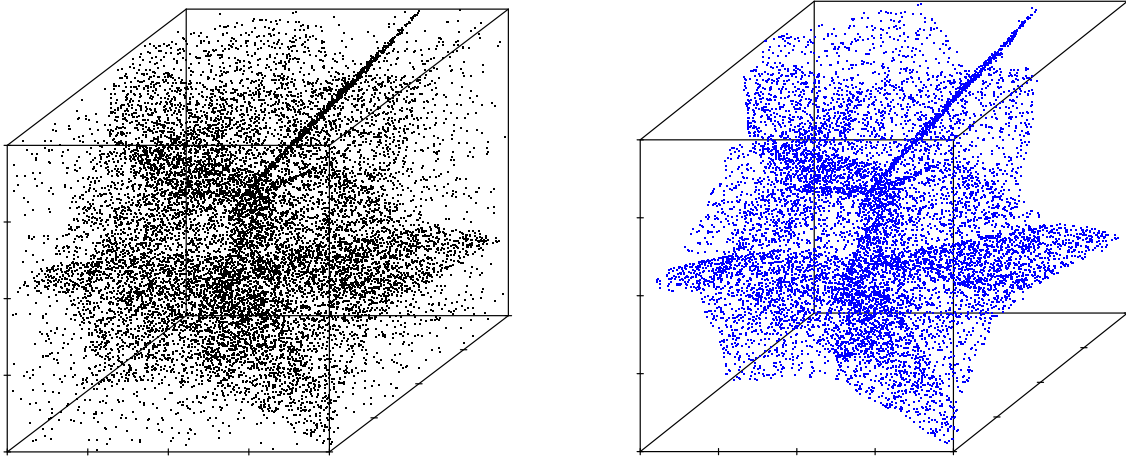


**Figure 15.** Left: data from a Voronoi foam model generating walls. Right: High signatures ridge points ( $d = 2$ ). Although it might be difficult to see in the plots, note that in the right plot the noise is gone and the walls remains.

By varying the proportion of points on these features one can control the amount of modes, filaments and walls. Finally, clutter points are added which are drawn from a uniform on  $[-1, 1]^3$ . We should point out that this is the simplest Voronoi foam model; more sophisticated versions that also include dynamics (moving galaxies) can be found in Icke and van de Weygaert (1991); van de Weygaert (1994); van de Weygaert and Schaap (2009). Figure 15 shows a dataset generated this way. In this example, we will focus on wall finding ( $d = 2$ ). To the best of our knowledge, there are no existing wall finding algorithms that actually output structures of dimensions  $d = 2$ . The right plot shows the result after filtering by the signatures. The blue points are the ridge points with a large signature. We see that the algorithm does a nice job of finding the dominant structures. It may be difficult to see in the plot, but in the right plot, the noise is gone and the walls remain.

## 6 Asymptotic Theory

Here we study the asymptotic properties of the procedure. We build on results from Genovese et al. (2014). To state the results, we need a few definitions and regularity conditions. Let

$H'(x) = d\text{vec}(H(x))/dx^T$  and let  $\lambda_1(x) \geq \dots \geq \lambda_D(x)$  be the ordered eigenvalues of  $H(x)$ . Let  $V(x)$  be the  $(D-d) \times D$  matrix with columns that are the  $D-d$  eigenvectors corresponding to the  $D-d$  smallest eigenvalue. Let  $L(x) = V(x)V(x)^T$  be the projection matrix corresponding to this subspace. Recall that  $R_d^\dagger(t) = \{x \in R_d : S_d(x) \geq t\}$ . Let  $B(x, r)$  denote a ball of radius  $r$  centered at  $x$ . Let

$$A \oplus r = \bigcup_{x \in A} B(x, r).$$

The Hausdorff distance  $\text{Haus}(A, B)$  between two sets  $A$  and  $B$  is defined by

$$\text{Haus}(A, B) = \inf \left\{ \epsilon : A \subset B \oplus \epsilon \text{ and } B \subset A \oplus \epsilon \right\}.$$

We assume there exist  $\beta, \delta, \epsilon, C > 0$  such that the following assumptions hold:

(A1)  $p$  is supported on a compact set  $\mathcal{X} \subset \mathbb{R}^D$  and is bounded and continuous and has five, bounded, continuous, square integrable derivatives. The first, second and third derivatives of  $p$  vanish on the boundary of  $\mathcal{X}$ .

(A2) The kernel  $K$  satisfies the regularity conditions in Giné and Guillou (2002), Arias-Castro et al. (2013) and Chacón et al. (2011).

(A3) For all  $x \in R_d \oplus \delta$ ,  $\lambda_{d+1}(x) < -\beta$  and  $\lambda_d(x) - \lambda_{d+1}(x) > \beta$ .

(A4) For each  $x \in R_d \oplus \delta$ ,

$$\|(I - L(x))g(x)\| \|\text{vec}(H'(x))\|_\infty < \frac{\beta^2}{2D^{3/2}}.$$

(A5) The eigenvalues  $\lambda_1(x), \dots, \lambda_D(x)$  are distinct.

(A6) Let  $T_d > 0$  be a fixed constant. For all  $-\epsilon < \gamma < \epsilon$  we have  $\text{Haus}(R_d^\dagger(T_d + \gamma), R_d^\dagger(t)) \leq C\gamma$ .

(A7) If  $x \in R_d$  but  $x \notin R_d \oplus \delta$ , then  $S_d(x) < T_d - \epsilon$ .

Assumptions (A1)-(A2) ensure the consistency of the estimates of the density and its derivatives. The regularity conditions on the kernel in (A2) are standard and we have not listed them to save space. Assumptions (A3) and (A4) are from Genovese et al. (2014). These conditions imply that the ridge is well defined. These assumptions are needed so that  $R_d$  can be estimated. Assumption (A5) is probably stronger than needed. It implies that the eigenvalues of the Hessian are continuously differentiable functions. It may be possible to relax this condition but the analysis would become much more complicated. (A6) says that the set  $R_d^\dagger(t)$  changes continuously in  $t$ . Condition (A7) says that points far from the ridge have a small signature.

Let us define

$$\psi_n = h^2 + \sqrt{\frac{\log n}{nh^{D+6}}}, \quad r_n = h^2 + \sqrt{\frac{\log n}{nh^{D+4}}}. \quad (15)$$

The following lemma follows from Lemma 3 of Arias-Castro et al. (2013) and Theorem 4 of Chacón et al. (2011).

**Lemma 1** Suppose that  $h \rightarrow 0$  and  $nh^{D+6}/\log n \rightarrow \infty$ . Assume (A1) and (A2) There exists  $0 < b < 1$  such that:

$$\sup_{(\log n/n)^{1/D} \leq h \leq b^{1/D}} \sup_{x \in \mathcal{X}} |\widehat{p}_h^{(\ell)}(x) - p^{(\ell)}(x)| \leq c_1 h^2 + c_2 \sqrt{\frac{\log n}{nh^{D+2\ell}}}$$

for  $\ell = 0, 1, 2, 3$ .

**Lemma 2** Assume (A1)-(A7). Suppose that  $h \rightarrow 0$  and  $nh^{2/(D+6)}/\log n \rightarrow \infty$ . Then

$$\sup_x |\widehat{S}_d(x) - S_d(x)| = O_p(r_n).$$

**Proof.** From Lemma 1,

$$\sup_x \max_{j,k} |\widehat{H}_{jk}(x) - H_{jk}(x)| = O_p(r_n).$$

Under the given assumptions,  $S_d(x)$  is a continuous, Lipschitz function of  $H$  and the result follows.  $\square$

**Theorem 3** Assume (A1)-(A7). Suppose that  $h \rightarrow 0$  and  $nh^{2/(D+6)}/\log n \rightarrow \infty$ . Then,

$$\text{Haus}(\widehat{R}_d^\dagger, R_d^\dagger) = O_p(\psi_n + r_n).$$

**Proof.** From conditions (A1)-(A4), we can conclude from Theorem 5 of Genovese et al. (2014) that  $\text{Haus}(\widehat{R}_d, R_d) = O_p(\psi_n)$ . Let  $x \in R_d^\dagger$ . Then, on an event with probability tending to one, there exists  $y \in \widehat{R}_d$  such that  $\|x - y\| \leq c\psi_n$  for some  $c > 0$ . Since  $x \in R_d^\dagger$ , we have that  $S_d(x) \geq T_d$ . From the previous lemma, and the fact that  $S_d$  is Lipschitz,

$$\widehat{S}_d(y) \geq S_d(y) - O_p(r_n) \geq S_d(x) - O_p(r_n) - O(\|x - y\|) \geq T_d - O_p(r_n) - O(\psi_n) \geq T_d - O_p(r_n + \psi_n).$$

Thus,  $y \in \widehat{R}_d^\dagger(T_d - O_p(r_n + \psi_n))$ . This shows that

$$R_d^\dagger(T_d) \oplus O_p(\psi_n) \subset \widehat{R}_d^\dagger(T_d - O_p(\psi_n + r_n)).$$

By a similar argument,

$$\widehat{R}_d^\dagger(T_d + O_p(\psi_n + r_n)) \subset R_d^\dagger(T_d) \oplus O_p(\psi_n).$$

From (A6), we conclude that

$$\text{Haus}(\widehat{R}_d^\dagger, R_d^\dagger) = O_p(r_n + \psi_n).$$

$\square$

Next, we find the asymptotic distribution and standard error of  $\widehat{S}_d(x)$ . This is useful for forming tests or confidence intervals for  $S_d(x)$ .

**Theorem 4** Assume the conditions Theorem 3. At each point for which  $\min_j |\lambda_j(x)| > 0$  for  $x \in \mathbb{R}_d^+$ ,

$$\sqrt{nh^{(D+4)/2}}(\widehat{S}_d(x) - \mathbb{E}[\widehat{S}_d(x)]) \rightsquigarrow N(0, \Gamma)$$

where

$$\Gamma = J_s J_\lambda \Sigma(x) J_\lambda^T J_s^T,$$

$\Sigma(x)$  is given in (16),  $J_\lambda$  is given in (19) and  $J_s$  is given in (20), (21), (22) and (23). If  $h = o(n^{-1/(D+4)})$  then

$$\sqrt{nh^{(D+4)/2}}(\widehat{S}_d(x) - S_d(x)) \rightsquigarrow N(0, \Gamma).$$

**Proof.** Theorem 3 of Duong et al. (2008) show that

$$\sqrt{nh^{(D+4)/2}}(\text{vech}(\widehat{H}(x)) - \mathbb{E}[\text{vech}(\widehat{H}(x))]) \rightsquigarrow N(0, \Sigma(x))$$

where

$$\Sigma(x) = R(\text{vech} \nabla^{(2)} K) p(x) \tag{16}$$

where  $R(g) = \int g(x)g(x)^T dx$  and  $\text{vech}$  is the half-vectorizing operator that stacks the upper triangular portion of a matrix into a vector. The condition  $\min_j |\lambda_j(x)| > 0$  together with (A5) implies that  $S_d(x)$  is continuously differentiable of  $H$ . Hence, the result follows from the delta method. It remains to find  $\Gamma$ .

By the delta method, the asymptotic covariance of  $S_d(x)$  is  $T = J_s \text{Cov}(\widehat{\lambda}) J_s^T$  where  $\text{Cov}(\widehat{\lambda})$  is the asymptotic covariance of  $\widehat{\lambda}$  and  $J_s$  the  $D \times D$  Jacobian of the signature function. Now  $\text{Cov}(\widehat{\lambda}) J_\lambda \Sigma J_\lambda$  where  $J_\lambda$  is the  $D \times D^2$  Jacobian of the eigenvalue. So  $\Gamma = J_s J_\lambda \text{Cov}(\widehat{\lambda}) J_\lambda^T J_s^T$ .

The signature vector  $S = (S_0, \dots, S_{D-1})$  is function of the vector  $\lambda$ , which is function of the Hessian. We can write

$$S = s(\lambda) \quad \text{with} \quad s : \mathbb{R}^D \mapsto \mathbb{R}^D \tag{17}$$

$$\lambda = \ell(\text{vec}(H)) \quad \text{with} \quad \ell : \mathbb{R}^{D^2} \mapsto \mathbb{R}^D. \tag{18}$$

From Chapter 8.8 of Magnus and Neudecker (1988),

$$J_\lambda = (u_1 \otimes u_1 \mid \dots \mid u_D \otimes u_D)^T \tag{19}$$

where  $u_j$  is the normalized eigenvector associated with  $\lambda_j$ .

Next we compute  $J_s$ . By direct computation, the terms below the diagonal of the Jacobian are the partial derivatives of  $S_j$  with respect to  $\lambda_1, \dots, \lambda_j$ :

$$\frac{\partial S_j}{\partial \lambda_k} = S_j \cdot \frac{I(\lambda_k < 0)}{\lambda_k - \lambda_D} \tag{20}$$

if  $\lambda_{j+1} < 0$  and  $\lambda_k < 0$  and is 0 if  $\lambda_{j+1} \geq 0$  or  $\lambda_k \geq 0$ . The terms on the diagonal, excluding the last one, are the partial derivatives of  $S_j$  with respect to  $\lambda_{j+1}$  for  $j = 0, \dots, D - 2$ :

$$\frac{\partial S_j}{\partial \lambda_{j+1}} = S_j \cdot \frac{2}{\lambda_{j+1}} \quad (21)$$

if  $\lambda_{j+1} < 0$  and 0 otherwise. Finally we consider the terms in the last column. For  $j < D - 1$ ,

$$\frac{\partial S_j}{\partial \lambda_D} = S_j \cdot \left( \frac{-1}{\lambda_D} + \frac{1}{\lambda_D} \sum_{i=1}^j \frac{\lambda_i}{\lambda_D - \lambda_i} I(\lambda_i < 0) \right) \quad (22)$$

Also,

$$\frac{\partial S_{D-1}}{\partial \lambda_D} = S_{D-1} \cdot \left( \frac{1}{\lambda_D} + \frac{1}{\lambda_D} \sum_{i=1}^{D-1} \frac{\lambda_i}{\lambda_D - \lambda_i} I(\lambda_i < 0) \right). \quad (23)$$

The last statement follows since, when  $h = o(n^{-1/(4+d)})$ , the squared bias is smaller than the variance.  $\square$

## 7 Discussion

We have presented a method for finding features of various dimensions. The method combines density ridge estimation with eigensignatures. There are several important problems that deserve further research.

First, we do not have a universal, data-driven method for choosing the tuning parameters. Although we have presented some heuristics for choosing the tuning parameters that seem to work well, it would be nice to have a truly data-driven method. Of course, the same is true for all structure finding methods that we are aware of. For example, spectral clustering methods involve numerous tuning parameters and so far there does not seem to be refined, principled methods for choosing the parameters. Indeed, even in simple clustering methods like  $k$ -means, there is no consensus on what is a good method for choosing  $k$ . This is an endemic problem in unsupervised methods.

Second, it will be interesting to investigate the use of our methods in high dimensions. In principle, the method can be used in any dimension. Of course, we expect it will be challenging to get good results in very high dimensions. Indeed, it is well known that the minimax rate for estimating densities degrades quickly with dimension. However, this does not make the problem hopeless. In high dimensions, we could lower our expectations and try to find only very prominent features. Specifically, let  $p_h$  be the mean of the density estimator with bandwidth  $h$ . We expect strong features to be present in  $p_h$  even if we do not let  $h$  tend to 0. And if we keep  $h$  bounded away from 0, then we can estimate  $p_h$  at rate  $O(1/n)$  independent of dimension. This suggests that finding singular features may be feasible in high dimensions although, at this point, this is merely a conjecture. But, perhaps the biggest challenge here,

is finding a way to visualize the results. It would be intriguing, for example, to find a  $d = 6$  dimensional feature in a  $D = 20$  dimensional dataset. But currently we have no way of visualizing a six-dimensional feature. Once again, this problem is not specific to our method; it is a very general problem in statistics and machine learning. Two promising methods for visualizing higher dimensional features are persistence diagrams (Chazal and Oudot (2008)) which is a two-dimensional plot summarizing the the topological features of a set and parallel coordinate plots (Wegman (1990)) which can be used to visualize data in any dimension.

Third, it would be useful to have a formal significance test to see if a structure is real. The asymptotic theory in Section 6 is a first step in this direction but so far we have no formal hypothesis test.

Fourth, it is not uncommon, when using clustering methods, to examine their stability properties. For example, one can make several splits of the data and compare the clusterings. A referee has suggested that a similar analysis would be useful here. We agree that this would be useful and the stability properties of singular feature finding should be further investigated.

Finally, the theory supporting the method is built on the theory in Chen et al. (2015b) and Genovese et al. (2014). But the theory in those papers is somewhat restricted. Certain regularity assumptions are assumed there that do not seem to be needed. For example, much of the theory assumes that the ridges do not intersect. And yet, we have seen in examples that the method works well in practice even if there are such intersections. Thus it would be useful to extend the theory to handle these situations.

## References

- Saeid Amiri, Bertrand Clarke, Jennifer Clarke, and Hoyt A. Koepke. A general hybrid clustering technique. *arXiv:1503.01183*, 2015.
- Ery Arias-Castro, David Mason, and Bruno Pelletier. On the estimation of the gradient lines of a density and the consistency of the mean-shift algorithm. Technical report, IRMAR, 2013.
- Peter Bubenik and Peter T. Kim. A statistical approach to persistent homology. *Homology, Homotopy and Applications*, 9(2):337–362, 2007.
- B. Cadre. Kernel estimation of density level sets. *Journal of multivariate analysis*, 97(4): 999–1023, 2006.
- Gunnar Carlsson. Topology and data. *Bulletin of the American Mathematical Society*, 46(2): 255, 2009.
- Gunnar Carlsson and Afra Zomorodian. The theory of multidimensional persistence. *Discrete & Computational Geometry*, 42(1):71–93, 2009.
- Marius Cautun, Rien van de Weygaert, and Berard JT Jones. Nexus: Tracing the cosmic web connection. *Monthly Notices of the Royal Astronomical Society*, 429.2:1286–1308, 2013.

- Chacón. Clusters and water flows: a novel approach to modal clustering through morse theory. *arXiv preprint arXiv:1212.1384*, 2012.
- J.E. Chacón, T. Duong, and MP Wand. Asymptotics for general multivariate kernel density derivative estimators. *Statistica Sinica*, 21:807–840, 2011.
- F. Chazal, L.J. Guibas, S.Y. Oudot, and P. Skraba. Persistence-based clustering in Riemannian manifolds. In *Proceedings of the 27th annual ACM symposium on Computational geometry*, pages 97–106. ACM, 2011.
- Frédéric Chazal and Steve Y. Oudot. Towards persistence-based reconstruction in euclidean spaces. In *Proceedings of the twenty-fourth annual symposium on Computational geometry*, pages 232–241. ACM, 2008.
- Yen-Chi Chen, Christopher Genovese, and Larry Wasserman. Enhanced mode clustering. *arXiv:1406.1780*, 2014.
- Yen-Chi Chen, Christopher Genovese, and Larry Wasserman. Statistical inference using the Morse-Smale complex. *arXiv preprint arXiv:1506.08826*, 2015a.
- Yen-Chi Chen, Christopher R Genovese, and Larry Wasserman. Asymptotic theory for density ridges. *Annals of Statistics*, To appear, 2015b.
- Yen-Chi Chen, Shirley Ho, Peter Freeman, Chris Genovese, and Larry Wasserman. Cosmic web reconstruction through density ridges: Method and algorithm. *arXiv:1501.05303*, 2015c.
- David Cohen-Steiner, Herbert Edelsbrunner, and John Harer. Stability of persistence diagrams. In *Proc. of the 21<sup>st</sup> Annu. Symp. Comput. Geom.*, pages 263–271, New York, June 2005. Assoc. of Computing Machinery. ISBN 1-58113-991-8. doi: <http://doi.acm.org/10.1145/1064092.1064133>. Symposium held in Pisa, Italy.
- D. Comaniciu and P. Meer. Mean shift: a robust approach toward feature space analysis. *Pattern Analysis and Machine Intelligence, IEEE Transactions on*, 24(5):603–619, may 2002. ISSN 0162-8828. doi: 10.1109/34.1000236.
- Maxime Descoteaux, Louis Collins, and Kaleem Siddiqi. A multi-scale geometric flow for segmenting vasculature in MRI. In *Computer Vision and Mathematical Methods in Medical and Biomedical Image Analysis*, pages 169–180. Springer, 2004.
- L. Dümbgen and G. Walther. Multiscale inference about a density. *The Annals of Statistics*, 36(4):1758–1785, 2008.
- Tarn Duong, Arianna Cowling, Inge Koch, and MP Wand. Feature significance for multivariate kernel density estimation. *Computational Statistics & Data Analysis*, 52(9):4225–4242, 2008.



- David Eberly. *Ridges in image and data analysis*, volume 7. Springer Science & Business Media, 1996.
- Herbert Edelsbrunner and John Harer. Persistent homology—a survey. *Contemporary mathematics*, 453:257–282, 2008.
- Herbert Edelsbrunner and John Harer. *Computational Topology: An Introduction*. Amer Mathematical Society, 2010.
- Herbert Edelsbrunner, David Letscher, and Afra Zomorodian. Topological persistence and simplification. *Disc. and Compu. Geom.*, 28(4):511–533, July 2002.
- Alejandro F Frangi, Wiro J Niessen, Koen L Vincken, and Max A Viergever. Multiscale vessel enhancement filtering. In *Medical Image Computing and Computer-Assisted Intervention—MICCAI-98*, pages 130–137. Springer, 1998.
- Patrizio Frosini. Discrete computation of size functions. *Journal of Combinatorics, Information and System Sciences*, 17(3-4):232–250, 1992.
- Keinosuke Fukunaga and Larry D. Hostetler. The estimation of the gradient of a density function, with applications in pattern recognition. *IEEE Transactions on Information Theory*, 21:32–40, 1975.
- Christopher Genovese, Marco Perone-Pacifico, Isabella Verdinelli, and Larry Wasserman. Nonparametric inference for density modes. *Journal of the Royal Statistical Society B.*, 2015.
- Christopher R. Genovese, Marco Perone-Pacifico, Isabella Verdinelli, and Larry Wasserman. Nonparametric ridge estimators. *The Annals of Statistics*, 42(4):1511–1545, 2014.
- Robert Ghrist. Barcodes: the persistent topology of data. *Bulletin-American Mathematical Society*, 45(1):61, 2008.
- E. Giné and A. Guillaou. Rates of strong uniform consistency for multivariate kernel density estimators. In *Annales de l’Institut Henri Poincaré (B) Probability and Statistics*, volume 38, pages 907–921. Elsevier, 2002.
- F Godtliebsen, JS Marron, and Probal Chaudhuri. Significance in scale space for bivariate density estimation. *Journal of Computational and Graphical Statistics*, 11(1):1–21, 2002.
- Vincent Icke and Rien van de Weygaert. The galaxy distribution as a voronoi foam. *Quarterly Journal of the Royal Astronomical Society*, 32:85–112, 1991.
- M.C. Irwin. *Smooth dynamical systems*, volume 94. Academic Press, 1980.
- George Karypis, Eui-Hong Han, and Vipin Kumar. Chameleon: Hierarchical clustering using dynamic modeling. *Computer*, 32(8):68–75, 1999.

- J. Klemela. *Smoothing of multivariate data: density estimation and visualization*, volume 737. Wiley, 2009.
- J. Li, S. Ray, and B.G. Lindsay. A nonparametric statistical approach to clustering via mode identification. *Journal of Machine Learning Research*, 8(8):1687–1723, 2007.
- X. Magnus and H. Neudecker. *Matrix differential calculus*. New York, 1988.
- Ozertem and Erdogmus. Locally defined principal curves and surfaces. *Journal of Machine Learning Research*, 12:1249–1286, 2011.
- W. Polonik. Measuring mass concentrations and estimating density contour clusters-an excess mass approach. *The Annals of Statistics*, pages 855–881, 1995.
- Wanli Qiao and Wolfgang Polonik. Theoretical analysis of nonparametric filament estimation, 2014.
- Sam T Roweis and Lawrence K Saul. Nonlinear dimensionality reduction by locally linear embedding. *Science*, 290(5500):2323–2326, 2000.
- Scott. *Multivariate density estimation. Theory, practice and visualization, first edition*. New York: John Wiley & Sons., 1992.
- Scott. *Multivariate density estimation: theory, practice, and visualization. Second edition*. John Wiley & Sons, 2015.
- Ali Snedden, Lara Arielle Phillips, Grant J Mathews, Jared Coughlin, In-Saeng Suh, and Aparna Bhattacharya. A new multi-scale structure finding algorithm to identify cosmological structure. *arXiv preprint arXiv:1409.7711*, 2014.
- Joshua B Tenenbaum, Vin De Silva, and John C Langford. A global geometric framework for nonlinear dimensionality reduction. *Science*, 290(5500):2319–2323, 2000.
- Katharine Turner, Yuriy Mileyko, Sayan Mukherjee, and John Harer. Frechet means for distributions of persistence diagrams. *arXiv preprint arXiv:1206.2790*, 2012.
- Rien van de Weygaert. Fragmenting the universe. 3: The constructions and statistics of 3-d voronoi tessellations. *Astronomy and Astrophysics*, 283:361–406, 1994.
- Rien van de Weygaert and Willem Schaap. The cosmic web: geometric analysis. In *Data Analysis in Cosmology*, pages 291–413. Springer, 2009.
- G. Walther. Granulometric smoothing. *The Annals of Statistics*, pages 2273–2299, 1997.
- Edward J Wegman. Hyperdimensional data analysis using parallel coordinates. *Journal of the American Statistical Association*, 85(411):664–675, 1990.
- Shi Zhong and Joydeep Ghosh. A unified framework for model-based clustering. *The Journal of Machine Learning Research*, 4:1001–1037, 2003.